

A preliminary study on pipe wall thinning of metallic underground utilities using in-pipe infrared thermography

by Samuel Yu*, Marco Kin Pan Ho, Wallace Wai-lok Lai, Janet Fung Chu Sham, Ho Chun You**

*Department of Land Surveying and Geo-informatics, The Hong Kong Polytechnic University, Hong Kong, samuel-yu.yu@connect.polyu.hk

**The Hong Kong and China Gas Company, Hong Kong

Abstract

Underground utilities are often prone to damage due to aging and external factors in which external corrosion has been reported as the main reason for pipe failure. Thus, obtaining the thickness of the pipe wall of the existing pipeline is crucial to prevent pipe failure. This study assesses the thermal signature of wall thinning in ductile iron pipes due to elevated temperature at reduced path length (or pipe wall thickness) of thermal transfer. It is a common problem that is caused by external corrosion in hostile underground environment. A new ductile iron pipe was prepared by milling several thinned regions of various sizes, shapes, and residual thicknesses onto the external wall. Wall thinning was investigated by infrared thermography using hot air as a heat source with the aid of visual images. Infrared and visual images of the inner pipe wall during a 2-minute heating phase were captured at a frequency of 9 Hz. While pipe interior surface feature could be eliminated by its sharp thermal response, thinned area generally has blurry boundary with a 0.5 °C temperature contrast with the sounded region. Therefore, a rapid condition assessment using infrared thermography for buried metal pipelines is successfully demonstrated.

1. Introduction

1.1. Background

Underground utilities served as the backbone of human society. They are infrastructures that transfer necessities and residuals such as water resources, natural gas, electricity, and sewage in and out of our premises. These underground infrastructures are high in density in most metropolises. Nevertheless, as for all infrastructures, they have limited-service lifetime due to natural deterioration from ageing and environmental factors such as corrosions; hence it is important to regular inspect and assess their conditions to ensure their serviceability throughout their lifecycle [1]. Without condition assessment, accident will occur without signals and warnings. For instance, water leakage from water-carrying pipelines leads to soil corrosion and results in sudden road collapsing and landslides [2, 3], or gas leakage from gas-carrying pipelines leading to devastating explosion [4, 5]. These accidents not only disturb the everyday life of citizens such as interruption of resources, but also causing loss of life and properties. Regular inspection help monitoring the condition of utilities thus help engineers planning maintenances priorities and rehabilitation works to minimize the number of accidents occurs.

1.2. Common technologies for underground utilities inspection

Many technologies have been developed and applied for condition assessment of underground utilities in past decades. Systematic reviews [6, 7] had been conducted in the past decade that summarized the methods of active pipe inspection of different types of underground utilities based on their working principle including visual inspection, electromagnetic methods, acoustic methods, ultrasound methods, radiography methods and thermography methods. Different methods provide different information of the inspected pipeline for decision making. However, only few can inspect the wall thickness of the underground utilities such as magnetic flux leakage, broadband electromagnetic, remote field eddy current, pulsed eddy current testing, Sahara system, phased array ultrasound technologies, radiography method and thermography methods [6, 7]. Nevertheless, these technologies have their own limitations to acquire the pipe wall thickness. Magnetic flux leakage testing and pulsed eddy current testing requires access of the external wall of the pipe [6, 7]; Broadband electromagnetic only works with pipelines made from ferrous materials and also requires access of the external wall of the pipe [8]; Remote field eddy current have weak detection signals for small pipe size [9] and without an external ferromagnetic ring, which are not applicable to onshore buried utilities, the sensitivity of the signals is weak [10]; Phase array ultrasound system requires a perfect contact, requires smoothing of the pipe surface which is hard to achieve if the pipe is not exposed, with the inspection surface [11]; Radiography methods requires an external film to record the results [6, 7] and traditional thermography methods requires an external heat source such as flash lamp to heat up the pipe to observe temperature variation and locating the thinned, in which both methods requires the pipe being exposed.

Despite the limitation of applying thermography methods in conducting condition assessments for underground pipelines, Sham, et al. [12] successfully conducted a condition assessment for two water carrying pipeline with pipe



diameter of 900 mm and 1800 mm which were rehabilitated respectively with high-density polyethylene (HDPE) liner and anchor knob sheet HDPE via in-pipe thermography using hot air as thermal stimulus. This is the earliest attempt in applying thermography without accessing the external pipe surface of the pipe and illustrates the potential of applying thermography methods in-pipe in conducting condition assessment for underground utilities without excavation. Nevertheless, without having any understandings of the difference in diagnosing air gap within the liner and in diagnosing the thickness of pipe wall, this paper, thus, presents a preliminary study of pipe wall thinning by applying in-pipe infrared thermography (IRT) techniques.

2. Material and Instrumentation

2.1. Test Sample

A testing site was set up buried with two ductile iron (DI) pipe manufactured according to British Standards Institution [13] with internal diameter of 300 mm and 400 mm respectively. The details of the pipes are listed in Table 1.

Table 1: Details of inspection

Details	Pipe Measurements	
	Nominal	Maximum Deviation
Internal diameter (mm)	400 mm	/
External diameter (mm)	429 mm	+1 mm -3.5 mm
Pipe Wall Thickness	~8.0 mm	-1.7 mm
Pipe length	1.5 m	



Fig. 1: Pipe sample with milled defects on the pipe exterior before buried attached with a flange connected to a riser pipe with shut off valve at the left of the pipe.

Fig. 1 shows the pipe used for this study before burying underground. One end of the pipe was plugged and attached to a riser which the hot air was transported into the pipe. The other end of the pipe was the entrance for the robotic tractor entering the pipeline for inspection. Each pipe was machine-milled with 36 flat-bottom holes on the pipe exterior. These holes had varying lateral size (25 mm, 50 mm, 75 mm) and residual thicknesses to imitate pit corrosion on a metallic pipe and were distributed on the pipe randomly into 6 rings in which each ring have 6 defects distributed in 6 directions - 12 o'clock, 2 o'clock, 4 o'clock, 6 o'clock, 8 o'clock and 10 o'clock with 12 o'clock in the zenith direction and 6 o'clock in the nadir direction. Each ring of defects, which represents the distance of that group of thinned area from the pipe entrance which Ring 1 is the closest to the entrance for the robot and Ring 6 is the furthest, was separated by approximately 208 mm to ensure the effect of diffusion in the longitudinal (z) direction is not affecting each other (Fig. 2). The design details on the pipe exterior for 400 mm pipe are listed in Table 2. The schematic drawings of the designed defects on both pipes are shown in Fig. 2. The defect notation (e.g. R6-75-l-4.0) is interpreted as the following:

- R1/2/3/4/5/6 – represents the ring number the defect locates;
- 25/50/75 – represents the lateral size of the defects in millimetre (mm);
- l/C/S – represents the defects in Peanut-shaped (l), Circle (C) or Square (S)
- 1.0-5.0 – represents the residual thickness of the defects measured by ultrasound probe

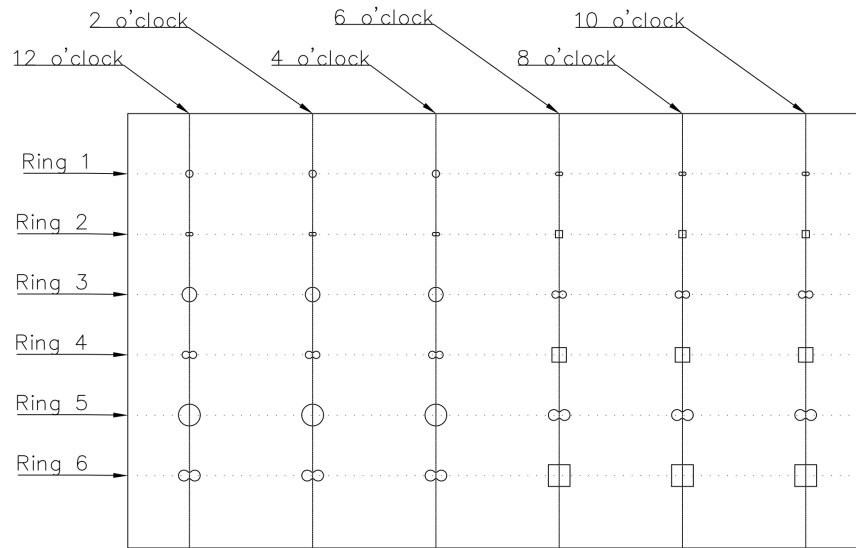


Fig. 2: Schematic drawings of the design defects on an unwrapped sheet

Table 2: Defect design details on the 400 mm DI pipe exterior

Angular Direction	Distance from entrance (mm)					
	208	416.7	625	833.3	1041	1250
12 o'clock	R1-25-C-2.1	R2-25-I-2.6	R3-50-C-3.5	R4-50-I-2.1	R5-75-C-2.2	R6-75-I-4.0
2 o'clock	R1-25-C-2.8	R2-25-I-4.0	R3-50-C-2.0	R4-50-I-2.7	R5-75-C-3.6	R6-75-I-1.7
4 o'clock	R1-25-C-4.0	R2-25-I-2.0	R3-50-C-2.8	R4-50-I-3.6	R5-75-C-2.0	R6-75-I-3.0
6 o'clock	R1-25-I-2.3	R2-25-S-3.1	R3-50-I-4.4	R4-50-S-2.1	R5-75-I-2.7	R6-75-S-4.0
8 o'clock	R1-25-I-2.7	R2-25-S-4.0	R3-50-I-2.0	R4-50-S-2.6	R5-75-I-4.0	R6-75-S-2.0
10 o'clock	R1-25-I-4.0	R2-25-S-1.8	R3-50-I-3.1	R4-50-S-4.0	R5-75-I-1.7	R6-75-S-2.6

2.2. Heat Source

In this study, active thermography was applied. A heat blower was set to 50 °C and was applied to the pipe as the source of heat. The heat blower was attached to the shut off valve at the end of the riser pipe as shown in Fig. 1., and the heating time has set to be 2 min.

2.3. Instrumentation

A heat blower was used for transport heat energy into the pipe (at $t = 0$ s). The change in temperature of the pipe interior surface was monitored by a long-wave infrared camera (7–14 μm) with a 640×512 pixel microbolometer at a frame rate of 9 Hz for 2 minutes after the heat blower started operating. The infrared camera is attached on a commercial class close circuit television (CCTV) robot. Due to the smaller pipe size compared to Sham, et al. [12], the infrared camera was not able to focus on to the crown on the pipe. Therefore, instead of having the infrared camera pointing perpendicular to

the crown of the pipe, a tunnel-view approach was adopted. Such approach also increases the inspection efficiency as the thermographic results of the whole pipe could be captured in one run. Since the length of the pipe specimen is only 1.5 m, the CCTV robot was staying still near the entrance of the pipe specimen for the whole 4 min from heating to cooling. The full set up of the test is shown in Fig. 3. The instrument specifications and parameters used for the acquisition of the thermogram are provided in Table 3.

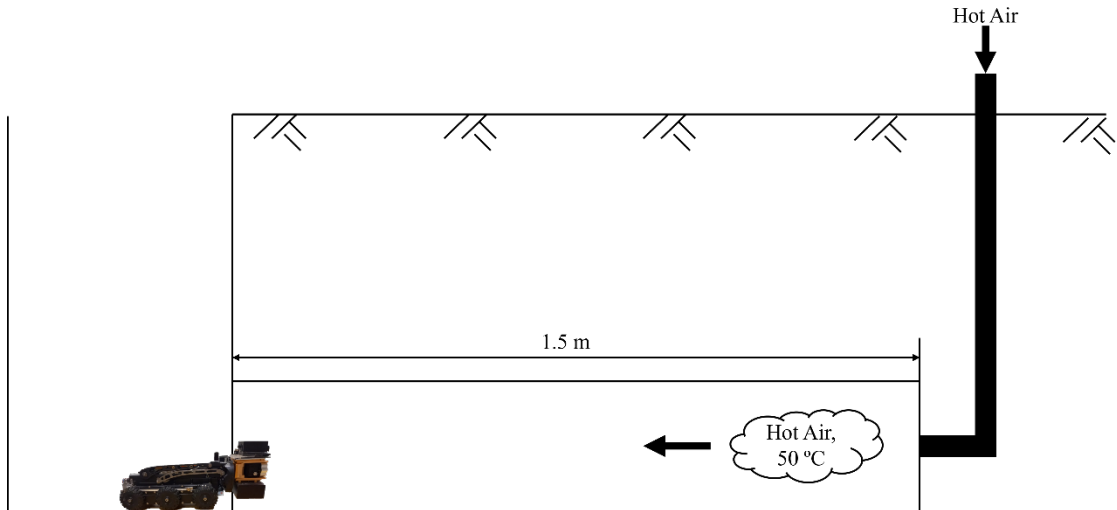


Fig. 3: Schematic diagram of on-site setup for active thermography

Table 3: Experimental equipment and acquisition parameters.

Experimental Equipment	Acquisition Parameters	
<i>Thermal stimulation:</i>	Sampling rate	9 Hz
Heat Blower	Acquisition duration	5 min
Heating duration: 5 min	Time interval	20 ms
<i>Thermographic monitoring</i>	Total number of frames	7800
TeAx Fusion, FOV (H×V) 47°×37°, 640 × 512 pixel microbolometer, 16-bit data, NETD: 50 mK, spectral range: 7.5-14.0 μm		

3. Result and Discussion

Fig. 4 is a thermogram in grey scale with the highest signal-to-noise ratio during the heating period with the white circle in the middle showing the hot air blown from the above ground and the black / grey circle being the attached flanged at the end of the pipe. Generally, the pixels that were high in temperature (white in colour) were considered as thermal anomalies which possibly mean defects. To distinguish interior defects from exterior corrosion, the blurry boundary characteristic of subsurface defects was used. Pipe interior defects such as soil deposits, encrustations, scales, and surface cracks usually having a sharp edge while thinned area could be treated as a subsurface defect usually having a blurry edge as thermal energy diffuse in three-dimension when traveling within the metallic medium.

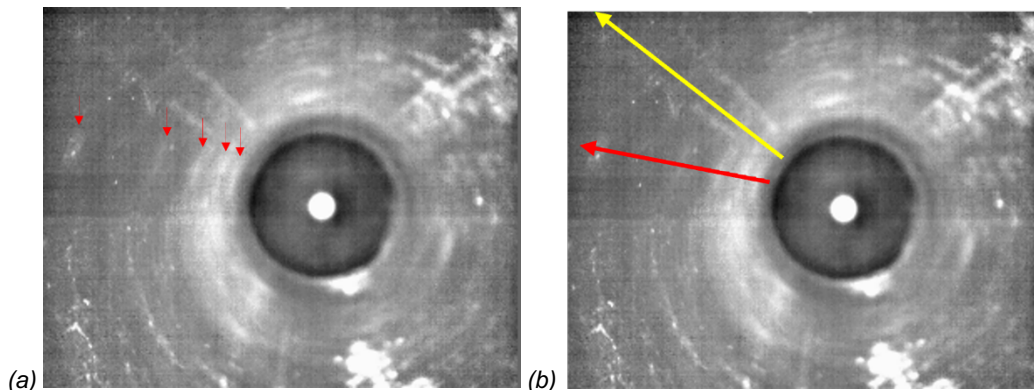


Fig. 4: (a) Thermogram at $t = 118$ s with a grayscale temperature bar ranging from 23.0 °C (black) to 24.7 °C (white) with red arrow indicating the thinned area in 10 o'clock angular direction; (b) Thermogram at $t = 118$ s with red and yellow arrow indicating the thinned area at 10 o'clock from ring 6 to ring 2 and the reference sound area respectively

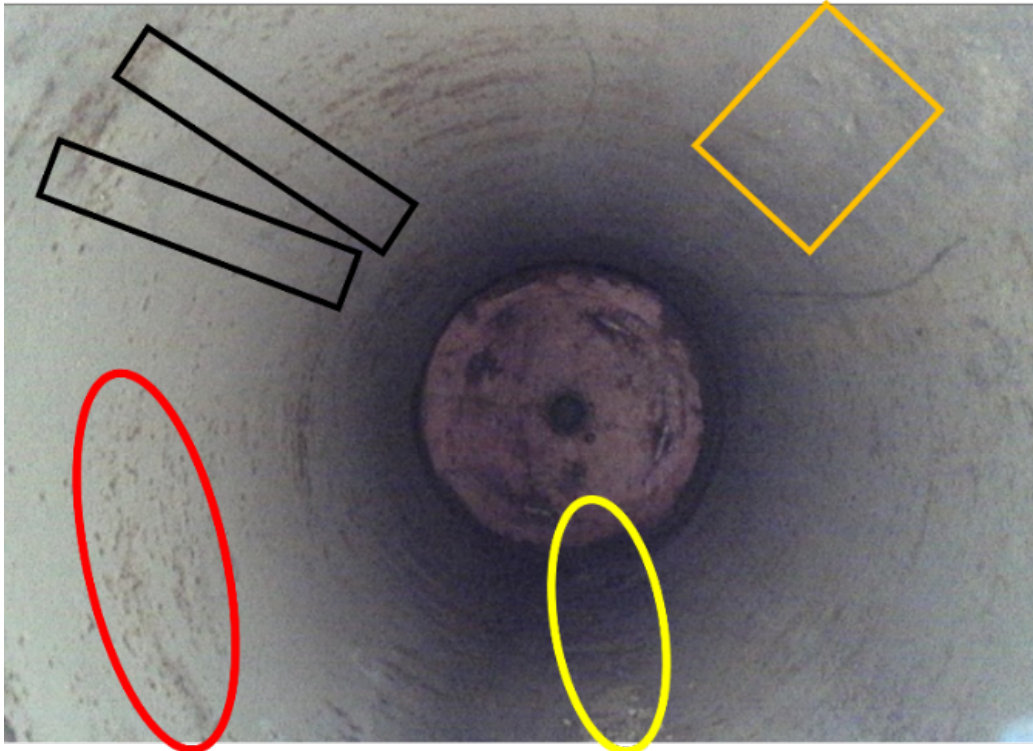


Fig. 5: Interior condition of the pipe specimen from optical image with annotated markings of possible surface features: Red oval: Scales, Yellow oval: Deposits, Black Rectangle: Welding Feature, Orange Rectangle: Surface Wear.

A thermal profile, shown in Fig. 6, from a chosen angular direction (10 o'clock) was plotted together with a thermal profile of sound area. The thermal profile in the angular direction of 10 o'clock was represented in red cross where the sound area was represented in blue square. In this thermal profile, it shows a general phenomenon of the further away from hot air source, the lower the temperature of the pipe wall it is. This is due to the nature of hot air dissipating when travelling through the pipe. Also, from Fig. 4, it is obvious that the left side of the pipe (from 12 – 7 o'clock) is generally hotter than the right side of the pipe. This may be due to the turbulence flow within the pipeline after exiting the small riser pipe into the pipe specimen. Thus, further studies on the heating process are recommended including possible pre-heating procedures or different thermal excitation source to solve the above-mentioned issue. Nevertheless, it is still observable that the thinned area can show a temperature difference of 0.5 °C compared with sound area.

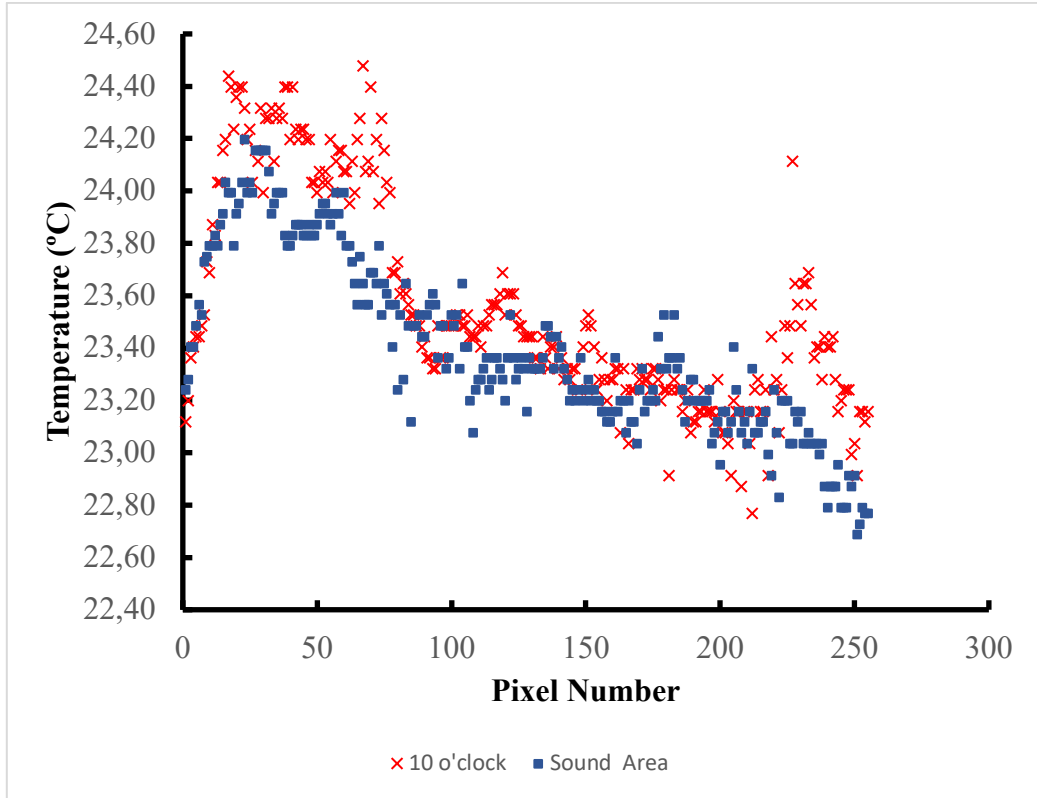


Fig. 6: Temperature Profile of the red cross and blue squares representing defective area and sound area respectively with 255 pixels extracted from Fig. 4

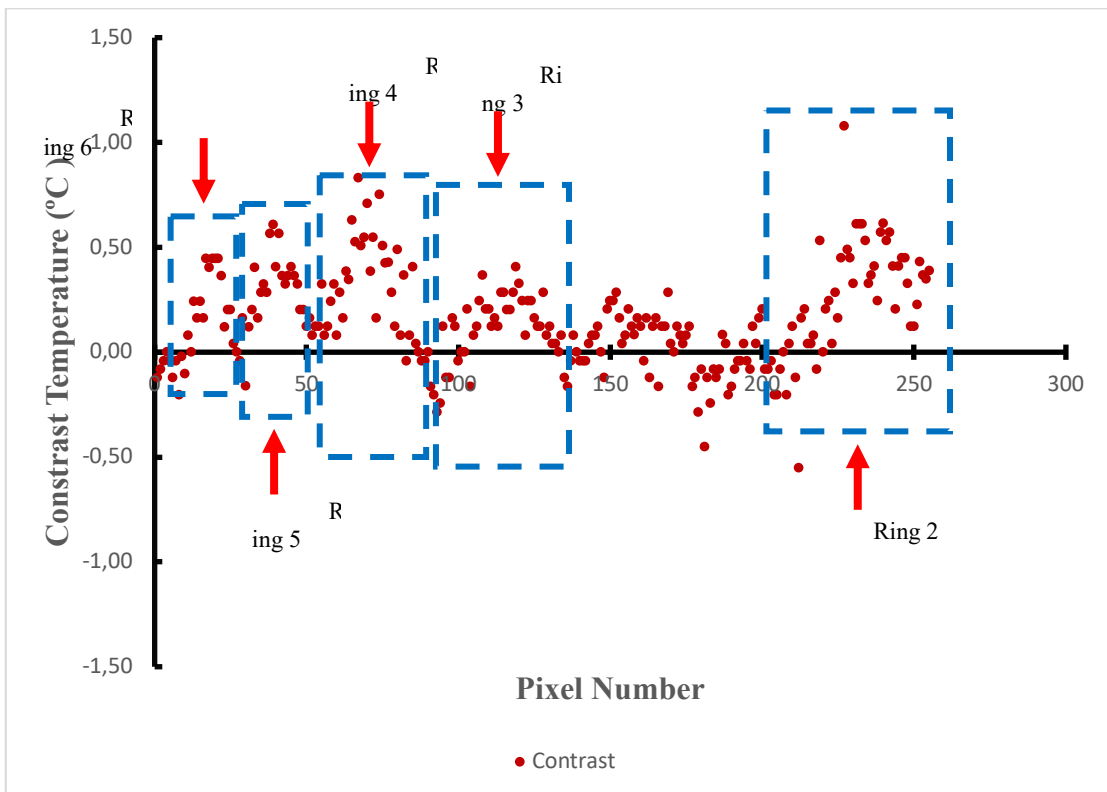


Fig. 7: Contrast of the temperature profiles from Fig. 6 corresponding to R6-75-S-2.6, R5-75-I-1.7, R4-50-S-4.0, R3-50-I-3.1 and R2-25-S-1.8 from left to right listed in row 10 o'clock listed in Table 2

4. Result and Discussion

This paper presents a pilot study on in-pipe active thermography for pipe wall thinning inspection and explored the application on in-pipe thermography for pipe wall thickness inspection. Infrared thermography inspection results shows that pipe interior surface feature generally have shaper thermal edges while thinned region have blurry edge in general with a 0.5 °C temperature contrast compared with sound region. Operating infrared camera in confined space with the use of hot air as heat source is challenging as it may overheat the infrared camera. Nevertheless, this study shows a prominent results of such application in pipe diagnosis even though more research should be conducted on the effect of heat dissipation of hot air to understand the effective heating distance and the computation of defect size in tunnel view to better quantify the defect characteristics.

5. Acknowledgement

The authors gratefully acknowledge the Hong Kong and China Gas Company Limited and the Innovation Technology Commission of the Government of the HKSAR for funding research project: Development of gas pipe diagnostic technology by nondestructive thermographic and ultrasonic methods (PRP/014/19FX).

REFERENCES

- [1] W. W.-L. Lai, "Underground Utilities Imaging and Diagnosis," in *Urban Informatics*, W. Shi, M. F. Goodchild, M. Batty, M.-P. Kwan, and A. Zhang Eds. Singapore: Springer Singapore, 2021, pp. 415-438.
- [2] C. Leung, "Underground water pipe bursts, triggers landslide in Hong Kong's upscale The Peak district," in *South China Morning Post*, ed. Hong Kong, 2021.
- [3] "Sinkhole caused by water mains burst claims victim - one minibus," in *The Standard*, ed. Hong Kong, 2022.
- [4] J. Hsu, E. Dou, and A. Poon, "Deadly Gas-Pipeline Explosions Rock Taiwan," in *The Wall Street Journal*, ed, 2014.
- [5] E. McKirdy and S. L. Erdman, "Dozens Dead as Taiwan Gas Explosions Tear Up Streets," in *CNN World*, ed. Taiwan, 2014.
- [6] J. Latif, M. Z. Shakir, N. Edwards, M. Jaszczkowski, N. Ramzan, and V. Edwards, "Review on condition monitoring techniques for water pipelines," *Measurement*, vol. 193, p. 110895, 2022/04/01/ 2022, doi: 10.1016/j.measurement.2022.110895.
- [7] Z. Liu and Y. Kleiner, "State of the art review of inspection technologies for condition assessment of water pipes," *Measurement*, vol. 46, no. 1, pp. 1-15, 2013/01/01/ 2013, doi: 10.1016/j.measurement.2012.05.032.
- [8] C. S. Feeney, S. Thayer, M. Bonomo, K. Martel, and D. Lai, "White Paper on Condition Assessment of Wastewater Collection Systems," U.S. Environmental Protection Agency, Washington, D.C., EPA/600/R-09/049, May 2009.
- [9] D. Zhou, X. Chang, Y. He, H. Wang, P. Cao, and L. Yang, "Influence of key factors on Eddy current testing sensitivity and monotonicity on subsurface depth for ferromagnetic and non-ferromagnetic materials," *Sensors and Actuators A: Physical*, vol. 278, pp. 98-110, 2018/08/01/ 2018, doi: 10.1016/j.sna.2018.05.018.
- [10] S. She, Y. Chen, Y. He, Z. Zhou, and X. Zou, "Optimal design of remote field eddy current testing probe for ferromagnetic pipeline inspection," *Measurement*, vol. 168, p. 108306, 2021/01/15/ 2021, doi: 10.1016/j.measurement.2020.108306.
- [11] Y. Yu, A. Safari, X. Niu, B. Drinkwater, and K. V. Horoshenkov, "Acoustic and ultrasonic techniques for defect detection and condition monitoring in water and sewerage pipes: A review," *Applied Acoustics*, vol. 183, p. 108282, 2021/12/01/ 2021, doi: <https://doi.org/10.1016/j.apacoust.2021.108282>.
- [12] J. F. C. Sham, W. W. L. Lai, W. Chan, and C. L. Koh, "Imaging and condition diagnosis of underground sewer liners via active and passive infrared thermography: A case study in Singapore," *Tunnelling and Underground Space Technology*, vol. 84, pp. 440-450, 2019/02/01/ 2019, doi: 10.1016/j.tust.2018.11.013.
- [13] Ductile iron pipes, fittings, accessories and their joints for gas pipelines — Requirements and test methods, EN 969:2009, British Standards Institution, London, 2009.